A&A 623, A170 (2019)
https://doi.org/10.1051/0004-6361/201833641

Astronomy & Astrophysics

Physical and dynamical properties of the unusual V-type asteroid (2579) Spartacus

Dagmara Oszkiewicz[1], Agnieszka Kryszczyńska[1], Paweł Kankiewicz[2], Nicholas A. Moskovitz[3], Brian A. Skiff[3], Thomas B. Leith[3], Josef Ďurech[4], Ireneusz Włodarczyk[5], Anna Marciniak[1], Stefan Geier[6,7], Grigori Fedorets[8], Volodymyr Troianskyi[1,9], and Dóra Föhring[10]

[1] Astronomical Observatory Institute, Faculty of Physics, A. Mickiewicz University, Słoneczna 36, 60-286 Poznań, Poland
e-mail: agn@amu.edu.pl
[2] Institute of Physics, Astrophysics Division, Jan Kochanowski University, Swietokrzyska 15, 25-406 Kielce, Poland
[3] Lowell Observatory, 14000 W Mars Hill Road, 86001 Flagstaff, AZ, USA
[4] Astronomical Institute, Faculty of Mathematics and Physics, Charles University, V Holešovičkách 2, 18000 Prague 8, Czech Republic
[5] Chorzów Astronomical Observatory MPC553, Chorzów, Polish Amateur Astronomical Society, Powstancow Wlkp. 34, 63-708 Rozdrazew, Poland
[6] Gran Telescopio Canarias (GRANTECAN), Cuesta de San José s/n, 38712 Breña Baja, La Palma, Spain
[7] Instituto de Astrofísica de Canarias, Vía Láctea s/n, 38200 La Laguna, Tenerife, Spain
[8] Department of Physics, Gustaf Hällströmin katu 2a, PO Box 64, 00014 University of Helsinki, Finland
[9] Astronomical Observatory of Odessa I.I. Mechnikov National University, Marazlievskaya 1v, 65014 Odessa, Ukraine
[10] Institute for Astronomy, University of Hawaii, 2680 Woodlawn Drive, Honolulu, HI 96822, USA

Received 14 June 2018 / Accepted 6 February 2019

ABSTRACT

Context. Asteroid (2579) Spartacus is a small V-type object located in the inner main belt. This object shows spectral characteristics unusual for typical Vestoids, which may indicate an origin deeper than average within Vesta or an origin from an altogether different parent body.
Aims. Our main goal is to study the origin of Spartacus. We derive the spin of Spartacus and a convex shape model of Spartacus in order to increase the knowledge of the body's physical properties. The rotational parameters are then used to investigate dynamical evolution of the object as well as to distinguish regions sampled by spectral observations to determine whether its surface displays heterogeneity.
Methods. We collected lightcurves available from the literature (oppositions of 2009, 2012) and obtained additional photometric observations at various telescopes in 2016, 2017, and 2018. We used the lightcurve inversion method to derive a spin and convex shape model. We have collected spectral observations over two rotational periods of Spartacus and determined its spectral parameters using the modified Gaussian model (MGM). We then dynamically integrated the orbital elements of Spartacus, taking into account existing information, including its thermal properties, size and the derived spin axis orientation.
Results. We find two models for (2579) Spartacus: (a) $\lambda = 312^\circ \pm 5^\circ$, $\beta = -57^\circ \pm 5^\circ$ and (b) $\lambda = 113^\circ \pm 5^\circ$, $\beta = -60^\circ \pm 5^\circ$ both retrograde. We find that the drift direction for Spartacus is consistent with separation from Vesta, and after a backward integration of 1 Gyr the asteroid reaches the boundary of the family. We did not observe spectral variations with rotation, thus the body most likely has a homogeneous surface. Additionally, new spectral analysis indicates that the 1.0 and 2.0 μm band centers are within ranges that are typical for Vestoids while the area ratio of these bands is about half that of typical Vestoids.
Conclusions. The asteroid (2579) Spartacus is in retrograde rotation and has a drift direction consistent with an origin from Vesta. The revised spectral band centers are within ranges typical for Vestoids, while band area ratio (BAR) is unusually low compared to that of other V-types. The dynamical model shows that the asteroid could have migrated to its current location from the edges of the Vesta family within 1 Gyr, but an origin from an earlier impact on Vesta could also be plausible.

Key words. minor planets, asteroids: individual: Spartacus – techniques: photometric – techniques: spectroscopic

1. Introduction

Most Howardite-Eucrite-Diogenite (HED) meteorites are thought to have originated from the crust of asteroid (4) Vesta. It is acknowledged that an impact on Vesta ejected debris and created V-type asteroids in the vicinity of Vesta, so-called Vestoids. Two large craters were discovered and mapped on the surface of Vesta (Thomas et al. 1997; Schenk et al. 2012) consistent with this scenario. Some of those ejected asteroids formed the Vesta family while others were scattered and drifted away though the Yarkovsky effect, encounters with other bodies and dynamical resonances (Scholl & Froeschlé 1991; Vokrouhlicky 1998; Vokrouhlický & Farinella 1999; Nesvorný et al. 2008; Carruba et al. 2007; Tsirvoulis & Novaković 2016) and are known as Vesta fugitives. Some were perturbed into near-Earth orbits, some of which later struck the Earth and were collected as meteorites. That evolutionary scenario has been now supported by multiple studies of meteorites and asteroids. However, a growing body of evidence suggests that Vesta might not be the only parent body of HED meteorites.

Most HED meteorites have similar oxygen isotope composition, which are indeed consistent with origin in a single body, (4) Vesta. However, some show distinct oxygen isotope ratios. This diversity in oxygen-isotope ratios coupled with other chemical ratios have clearly indicate that Vesta is almost certainly not the parent body of several meteorites. For example, meteorite NWA011 falls compositionally far from other HEDs and closer to the CR-chondrites (Yamaguchi et al. 2002; Floss et al. 2005). Several other meteorites: Ibitira, Caldera, Pasamonte, and ALHA78132 are ^{16}O-depleted compared to other eucrites (Wiechert et al. 2004). Another meteorite (Bunburra Rockhole) also shows a distinct oxygen isotope composition (Spurnỳ et al. 2012; Bland et al. 2009), and is particularly intriguing. The fall of this meteorite was observed and its origin was traced back to the inner asteroid belt (Bland et al. 2009) – a region predominantly populated by Vestoids. Yet, Bunburra Rockhole seems to have a non-Vestoid origin. There might, therefore, be as yet unidentified V-type asteroids in the inner main belt that are not fragments of (4) Vesta and thus represent parent bodies of the anomalous HED meteorites.

Several V-type asteroids (spectral analogs to HED meteorites) unlinkable to Vesta have been discovered in the mid and outer main belt (for example Lazzaro et al. 2000; Solontoi et al. 2012; Duffard & Roig 2009; Moskovitz et al. 2008; Roig et al. 2008; Oszkiewicz et al. 2014, and others). Due to the separation by the strong 3:1 resonance with Jupiter they cannot be easily dynamically connected to (4) Vesta. The spectral properties of these objects also differ from typical Vestoids (Ieva et al. 2016; Leith et al. 2017) strengthening the idea that these are not fragments of (4) Vesta (and are thus called non-Vestoids). Based on spectral properties and spatial distrubution Ieva et al. (2018) suggested at least two parent bodies (other then Vesta) for those objects. Dynamical studies (Carruba et al. 2014; Huaman et al. 2014) indicate seven source regions and thus seven possible parent bodies (or alternatively seven scattering events from Vesta). On the other hand, no V- or A-type asteroid clusters have been identified (DeMeo et al. 2019; Burbine et al. 2017) so far in the mid and outer main belt and the distribution of these bodies appears random. Brasil et al. (2017) suggest that the "jumping-Jupiter" planetary migration scenario could perhaps explain the existence of some of those V-types in the middle main belt. However, meteorite delivery to Earth from these distant regions is highly improbable, therefore these asteroids are unlikely source of the anomalous HEDs.

Generally the inner main belt is considered to be the main source region of meteorites. Oszkiewicz et al. (2015) and Oszkiewicz et al. (2017) show that some V-type prograde rotators in the inner main belt have Yarkovsky drift direction that is inconsistent with origin in the Vesta family and may represent parent bodies of those anomalous HEDs. Spectroscopic surveys of this region (Burbine et al. 2001; Moskovitz et al. 2010; Mayne et al. 2011) have yet to unambiguously identify V-type asteroids that are not related to Vesta.

However, mineralogical analyses of NIR spectra have identified a single candidate that may be an example of a non-Vesta V-type in the inner Main Belt: asteroid 2579 Spartacus. Spartacus is approximately 5 km in diameter and orbits near the periphery of the Vesta family. Burbine et al. (2001) found that the NIR spectrum of Spartacus indicated a composition more olivine-rich than that of typical Vestoids, with an implication being that Spartacus could sample a source region deeper within Vesta's crust or upper mantle. Moskovitz et al. (2010) quantitatively confirmed the unusual spectral properties of Spartacus, namely that it displays a much smaller band area ratio (ratio of the area enclosed in the 2 micron absorption band relative to area in the 1 micron band) than other Vestoids.

One model for Vestoid formation involves the re-accumulation of small (meter scale) fragments removed from Vesta's crust and upper mantle at the time of the family-forming collision (Eugster et al. 2006). However, in this scenario it is unclear how large amounts of Vesta's olivine-rich mantle could have preferentially re-accreted into a single body to form Spartacus, but did not do so for other Vestoids that have been studied spectroscopically. It is possible that Spartacus is a monolithic unit that was removed intact (Asphaug 1997). If this is the case then it may sample a compositional gradient across Vesta's crust and upper mantle, which could produce spectral variations across the surface. Alternatively, Spartacus could be unrelated to Vesta.

To address these issues we conducted a focused spectroscopic and photometric campaign to constrain the mineralogy of Spartacus, to determine whether its surface displays any compositional heterogeneity, and to determine its spin, shape, and dynamical properties. In the following sections we determine its spin and shape properties (Sect. 3), rotationally resolved spectral properties (Sect. 5) and use these to study dynamical evolution of this object (Sect. 6). As a whole these analyses are used to consider the possibility that Spartucus could be a parent body of unusual HED meteorites such as Bunburra Rockhole.

Table 1. Observing sites, dates of observations, and instrumentation used.

Date	IAU code	Telescope	Instrument
2016-Mar.-04	807	SMARTS	ANDICAM
2016-Mar.-09	807	SMARTS	ANDICAM
2016-Jul.-13	688	Hall	NASA42
2016-Jul.-27	807	SMARTS	ANDICAM
2016-Jul.-29	807	SMARTS	ANDICAM
2016-Aug.-08	688	Hall	NASA42
2017-Sep.-02	688	Hall	NASA42
2017-Sep.-28	950	NOT	ALFOSC
2018-Mar.-04	950	JKT	Andor Ikon-L

2. Photometric observations and data

Photometric observations were acquired at the 1.3 m SMARTS, 1.0 m Hall telescope, 2.5 m Nordic Optical Telescope (NOT) and 1.0 m *Jacobus Kapteyn* Telescope (JKT; Keel et al. 2016). Telescopes and instruments used are listed in Table 1.

All observations used CCD (charge-coupled device) cameras, and observations were collected in the V, R or Sloan r-band filters. The data reduction was done using the MPO Canopus or the Starlink package (Currie et al. 2014) for data from SMARTS, Hall, and NOT telescopes and IDL self-written codes for JKT data. Standard bias and flat-field corrections were applied. Data from JKT were additionally corrected for dark frames, as the camera was cooled only to −50 °C. Aperture photometry was performed to obtain differential magnitudes, observing times were corrected for light-time. We gathered a total of nine lightcurves in three different oppositions.

27 lightcurves in V and R bands were also downloaded from the ALCDEF database (11 from Dykhuis et al. 2016 and 16 by Moskovitz & Warner 2012). These observations spanned a range from 2009 to 2012. Collectively we used 36 lightcurves from five oppositions spanning 2009 up to 2018.

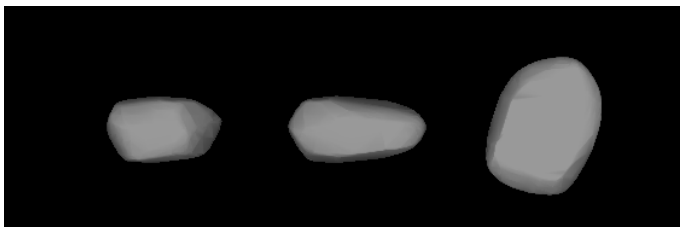

Fig. 1. Convex shape model of (2579) Spartacus: views along the X, Y, Z axis in the asteroid's cartesian frame. Pole coordinates are $\lambda = 312° \pm 5°$, $\beta = -57° \pm 5°$, rotational period $P_{\rm sid} = 3.636028$ h.

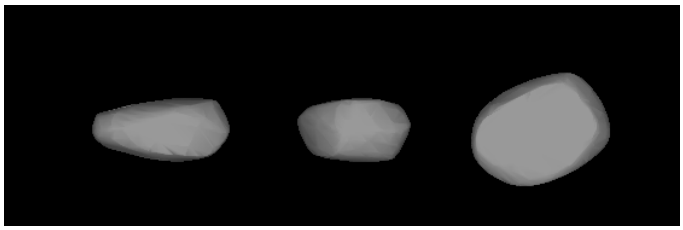

Fig. 2. As in Fig. 1, but for a symmetric pole solution $\lambda = 113° \pm 5°$, $\beta = -60° \pm 5°$, $P_{\rm sid} = 3.636027$ h.

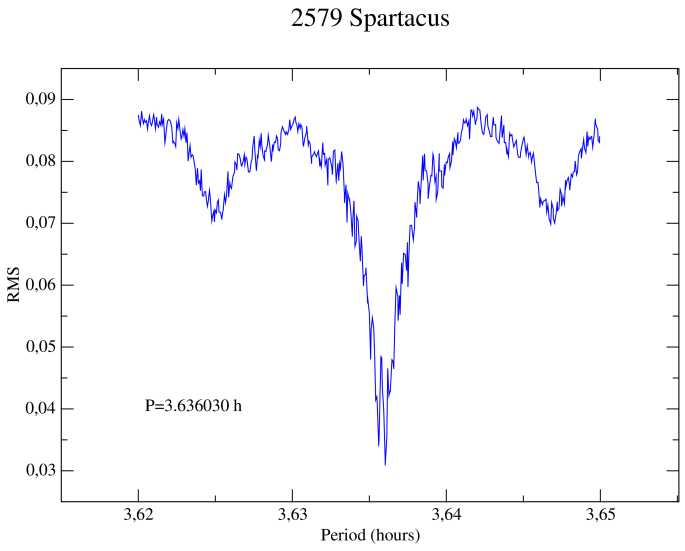

Fig. 3. Periodogram of sideral period for Spartacus.

3. Spin and convex shape model

The pole direction and convex shape models for (2759) Spartacus were obtained using the lightcurve inversion method by Kaasalainen & Torppa (2001) and Kaasalainen et al. (2001).

We used all the 36 lightcurves. One of the lightcurves due to a constant magnitude offset was split into two parts. We obtained a retrograde model with spin axis orientation $\lambda = 312° \pm 5°$, $\beta = -57° \pm 5°$ (Fig. 1) and a symmetric also retrograde solution $\lambda = 113° \pm 5°, \beta = -60° \pm 5°$ (Fig. 2). Periodogram of the sidereal period for Spartacus is shown in Fig. 3.

Retrograde rotation implies negative Yarkovsky drift, thus based on rotation only the origin in (4) Vesta can not be dynamically excluded for Spartacus. Efficiency of the Yarkovsky effect must be investigated to see whether the object could evolve from the location of Vesta to its current position within the last 1 Gyr (age of the Vesta family).

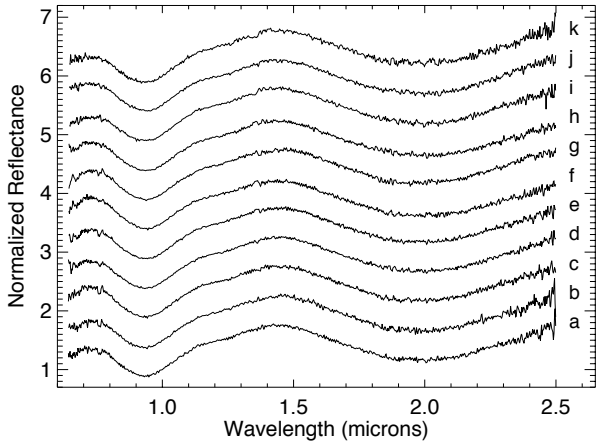

Fig. 4. SpeX time series spectra of 2579 Spartacus. Spectra are normalized at 1 micron and offset for clarity. The time series starts with spectrum "a" at 07:46 UT and continues through the spectrum labeled "k" at 13:55 UT on 2 February 2012. Typical signal-to-noise for each spectrum ranges from 50 to 100 across the wavelength range.

4. Spectral observations

To probe the previously reported spectral properies of Spartacus, near-infrared (NIR, 0.8–2.5 micron) spectroscopic observations were conducted between about 07:45 and 14:30 UT on 2 February 2012 at NASA's IRTF using the SpeX instrument (Rayner et al. 2003). SpeX was configured in its low resolution prism mode with a 0.8″ slit to produce wavelength coverage from 0.7 to 2.5 microns. The telescope was operated in a standard ABBA nod pattern with 120 s exposures per nod position.

A continuous series of spectra were obtained with approximately hourly interludes for observations of solar analog star HD 77730, which was located less than 15 degrees away from the asteroid. The geometric observing conditions for the asteroid remained essentially constant throughout the observing window with a solar phase angle of −2.4°, a geocentric distance of 1.30 AU, heliocentric distance of 2.29 AU, and an apparent magnitude of $V = 16$. The time series of spectra across six hours covered almost two full rotation periods.

Reduction of the spectral data employed the IDL-based Spextool package (Cushing et al. 2004). A custom telluric correction routine that leveraged the ATRAN atmospheric model (Lord 1992) was applied to spectra of both the asteroid and solar analog star. The full time series of normalized reflectance spectra are shown in Fig. 4. Each spectrum represents approximately 30 min of integration time.

5. Spectral analysis

We analyzed our collection of SpeX spectra with the modified Gaussian model (MGM; Sunshine et al. 1990). This approach followed that of Leith et al. (2017) in that MGM was used with as few free parameters (i.e. input bands) as possible in fits to spectra of pyroxene-rich mafic compositions. This approach involved a single set of input parameters to fit spectra of asteroids, meteorites, and synthetic pyroxenes, and produced consistent compositional results across these three groups of objects. We adopted here the same set of input MGM parameters to measure the 1 and 2 micron band centers and band area ratio (BAR = Band 2 area/Band 1 area) of the Spartacus data. These band centers allow us to constrain the composition of Spartacus and assess the extent of rotational spectral variability.

Table 2. Measured spectral properties for the labeled (a–k) spectra in Fig. 4. Rotational phase is given relative to UT 2012-02-02 at 07:46.

Spectrum	UT time	Rotational phase	B1 center	B2 center	BAR
a	07:46:24	0.00	0.931 ± 0.002	1.9750 ± 0.0001	1.44
b	08:31:59	0.21	0.931 ± 0.002	1.9752 ± 0.0001	1.34
c	09:16:03	0.41	0.933 ± 0.002	1.9719 ± 0.0001	1.42
d	09:49:12	0.56	0.933 ± 0.002	1.9794 ± 0.0001	1.48
e	10:25:56	0.73	0.934 ± 0.002	1.9758 ± 0.0001	1.43
f	11:11:49	0.94	0.936 ± 0.002	1.9828 ± 0.0001	1.62
g	11:45:55	0.10	0.935 ± 0.002	1.9743 ± 0.0001	1.45
h	12:26:59	0.29	0.935 ± 0.002	1.9991 ± 0.0001	1.69
i	12:56:50	0.42	0.933 ± 0.002	1.9825 ± 0.0001	1.51
j	13:28:30	0.57	0.936 ± 0.002	1.9825 ± 0.0001	1.79
k	13:54:55	0.69	0.932 ± 0.002	1.9792 ± 0.0001	1.54

Notes. One and two micron band centers (B1 and B2 center respectively) and band area ratio (BAR) are measured based on MGM fits to the data.

Our measured spectral band parameters are summarized in Table 2. Three sigma errors on the band centers were determined based on the empirical relationship derived by Leith et al. (2017) where Monte Carlo simulations were run to determine band center errors as a function of signal-to-noise ratios (S/N). We use the measured S/N of our spectra to estimate band center errors. As noted in Leith et al. (2017) these error bars are approximate and do not fully represent non-statistical error sources in the data (e.g. outlying points due to imperfect telluric correction). As such these errors may represent a lower limit. A similar empirical metric does not exist for BAR, thus we do not formally determine its error bars, but note that it shows significantly more scatter than the band centers with a one-sigma standard deviation across our data set of 0.13 (~10% as opposed to ~0.1% for the band centers).

To address the previously reported compositional results Burbine et al. (2001) and Moskovitz et al. (2010) we compare the MGM derived band centers of our new data to those of the previous Spartacus spectrum, Vesta, a selection of Vestoids, and a suite of HED meteorites (Fig. 5). Spectra for all of these objects were analyzed in an identical way, the results of which were taken directly from Leith et al. (2017). We find that the band centers of our newly presented spectra are fully consistent with other Vestoids and the suite of HED meteorites. These centers suggest pyroxene iron molar content $F_s \sim 36\%$, which is not unusual for Vestoids. The previously measured spectrum of Spartacus shows a similar B2 center but slightly lower B1 center. This difference could be attributed to uncontrolled systematics in the data acquisition or reduction of the earlier data.

Spartacus was originally identified by Burbine et al. (2001) as compositionally unusual based on an anomalously broad 1 micron absorption feature. Moskovitz et al. (2010) confirmed this quantitatively by showing that Spartacus has a BAR roughly half that of other Vestoids, and is the only inner Belt V-type asteroid with BAR < 1.8. The analysis of our new data confirm this unusual spectral signature; however, a detailed compositional interpretation of such a spectrum requires additional analysis. We suggest two possibilities in need of further investigation to explain the spectral properties of Spartacus. First, Spartacus could contain an enhanced abundance of olivine (Burbine et al. 2001). However, that would be somewhat surprising in light of an apparent lack of endogenous olivine on Vesta (Turrini et al. 2016). Alternatively, the pyroxenes on Spartacus may be rapidly cooled basaltic material, as opposed to slowly cooled cummulates, which has been shown to result in a strong 1.2 micron band

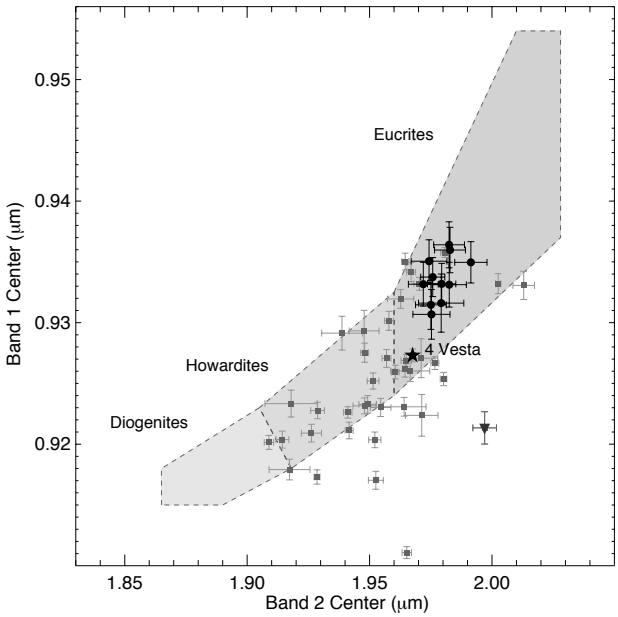

Fig. 5. Band diagram of MGM measured band centers for 2579 Spartacus (filled circles), 4 Vesta (star), and other Vestoids (gray squares). The regions occupied by the HED meteorites are included as determined by Leith et al. (2017) using the same methodology. A previous Spartacus spectrum from October 2000 is shown as the inverted triangle. The location of Spartacus in this diagram based on our new data is largely consistent with other Vestoids and most akin to a eucritic composition.

(Klima et al. 2008). A prominent 1.2 micron band would enhance the effective Band 1 area and thus decrease BAR.

Our data set and analysis has further enabled an investigation of surface heterogeneity on Spartacus. Figure 6 shows the time series of spectral parameters phased to the 3.63 h rotation period. Error bars on the band centers are as reported in Table 2. The error bars on BAR represent the 1-sigma standard deviation of all measured values. While some of the individual band parameter measurements do deviate from the mean value, the lack of such repeatability across multiple rotations suggests that these are not caused by physical properties on the surface, but instead by observational systematics. As such we find no clear evidence for surface heterogeneity on Spartacus and instead use the scatter in our data to place detection limits on such variability.

Additional analysis of our band parameters, namely calculation of the Pearson correlation coefficient, shows that B2 center and BAR are correlated at 99.5% significance, and B1 center and BAR are correlated at 99% significance. We believe these correlations are an artifact of the MGM fitting routine and not due to physical causes. If composition were driving a change in band parameters for this basaltic asteroid then we would expect B1 and B2 centers to be positively correlated (Fig. 5), instead they are only weakly correlated at 85% significance, and B1 and BAR to show essentially no correlation (e.g. Hardersen et al. 2018). We note that while these correlations are statistically significant, the changes, particularly in the band centers, are quite small and thus would have minor compositional implications.

6. Dynamical model

To study dynamical evolution of (2579) Spartacus we randomly generated 1001 clones with initial orbital elements distributed along the line of variation of orbital elements of (2579) Spartacus. Those clones were then integrated backwards

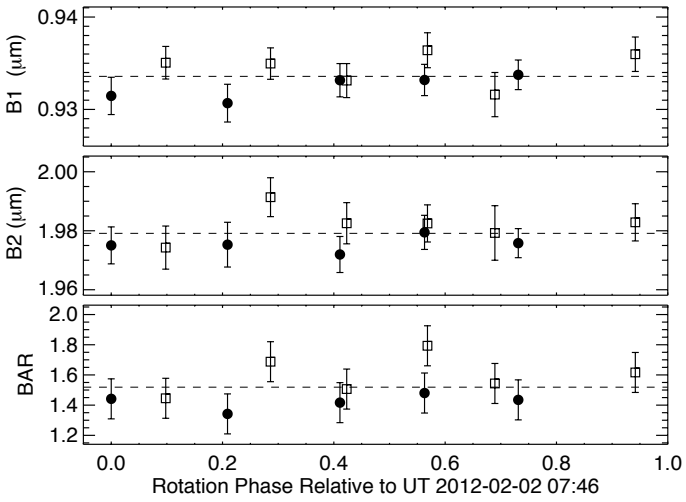

Fig. 6. Time series of spectral band parameters, phase folded to a period of 3.63 h. Spartacus was observed across nearly two full rotations, the first indicated by the filled circles, the second by the open squares. The mean for each parameter is represented by the dashed line. No repeatable variability was detected in any of the band parameters.

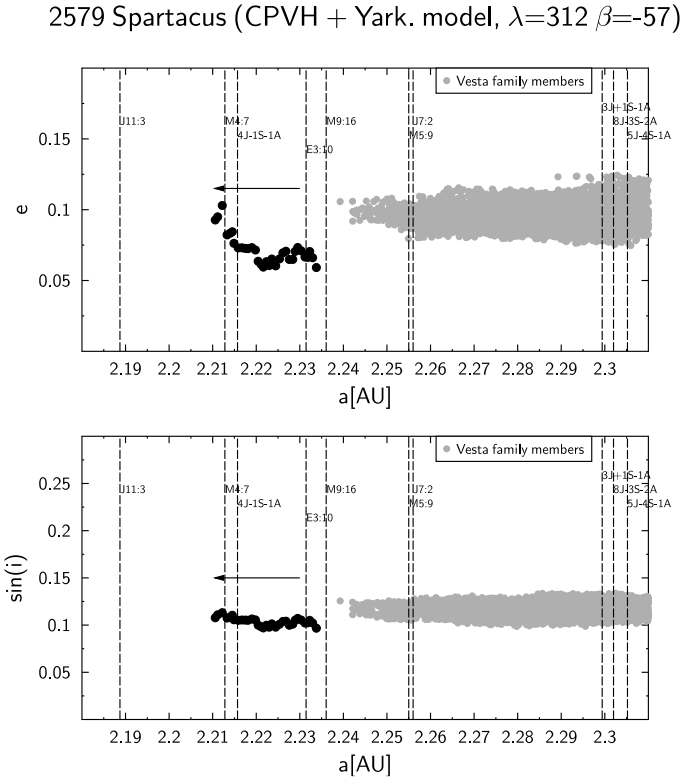

Fig. 7. Evolution of proper elements of Spartacus during 1 Gyr (spin orientation (a)). The direction of the Yarkovsky drift is marked by arrow.

in time for 1 Gyr (the approximate age of the Vesta family Spoto et al. 2015, Carruba & Nesvorný 2016) evolving under the influence of the Yarkovsky effect and interacting with the local web of resonances (mean-motion and secular). All the clones had a radius that of (2579) Spartacus, that is $r_S = 2.302$ km (Masiero et al. 2011). The initial thermal parameters were selected to resemble that of typical V-types asteroids (that is bulk density $\rho_{\rm bulk} = 3000$ (kg m^{-3}), surface density $\rho_{\rm surf.} = 1500$ (kg m^{-3}), thermal conductivity $\kappa = 0.001$ (W K^{-1} m^{-1}), thermal capacity $C = 680$ (J kg^{-1} K^{-1}), albedo $p_V = 0.5257$, infrared emissivity $\epsilon = 0.95$). We used the period $P = (3.636028\ \mathrm{h}, 3.636027\ \mathrm{h})$, and spin orientation $(a)\,(\lambda = 312°, \beta = -57°), (b)\,(\lambda = 113°, \beta = -60°)$ derived in Sect. 3. The dynamical model included gravitational forces including the Sun and eight planets (using the JPL DE405 planetary ephemeris), perturbations from Ceres, Pallas, Vesta, and Hygiea (Carruba et al. 2007; Tsirvoulis & Novaković 2016) indicate that the close encounters or secular resonances with Vesta could influence orbital evolution of bodies in the inner main belt) and the thermal Yarkovsky force (we refer to it as using CPVH model further in the text). We used `SWIFT_RMVSY` software package as the main tool of numerical integration and calculations of mean and proper elements. We computed the osculating elements, eliminate frequencies lower than 1000 yr and estimate proper elements using the `SWIFT_RMVSY` software package.

We have considered the two retrograde cases with the actual pole solutions derived in Sect. 3. Evolution of the proper orbital elements using the CPVH model for those cases is shown in Figs. 7 and 8 respectively. During the 1 Gyr evolution Spartacus crossed the region of 4J-1S-1A and M4:7 mean motion resonances.

To estimate the possible influence of close approaches to Ceres, Pallas, Vesta and Hygiea, we performed additional short-time (10^8 yr) integrations to compare models with and without the four massive asteroids. We detecte no close approaches to Ceres, ten to Pallas and 31 to Vesta[1]. The closest approaches we found were those to Vesta. We did not find any close encounters with Hygiea. The cumulative effect of the close approaches to Vesta was around 10^{-3} AU in proper semi-major axis during 10^8 yr. For comparison the cumulative Yarkovsky effect was $\sim 5 \times 10^{-3}$ AU during the same time period.

We also analyzed resonances with Vesta, focusing on nodal precession and precession of line of apsides. Tsirvoulis & Novaković (2016) indicates their potential impact on asteroids in the vicinity of the Spartacus region (in particular the nodal resonance). We found no significant secular resonances. No such resonances for Spartacus were also found in Carruba et al. (2005). We cannot rule out the possibility that weak secular resonances (e.g. of a higher order) occur in the range of Spartacus orbital elements. However, we do not notice any visible effects of these resonances.

For both retrograde cases after 1 Gyr backward integration we find that the clones reach the border of the Vesta family, thus making it plausible that Spartacus dynamically evolved from (4) Vesta. Since the object reached only the edges of the family, the initial ejection velocity from Vesta had to be large or Spartacus separated from Vesta more than 1 Gyr ago, perhaps in an impact like the one that created the Veneneia crater with estimated age >2 Gyr.

7. Conclusions

Based on the collected multi-opposition data, we obtain two retrograde model solutions for asteroid (2579) Spartacus (rotational pole coordinates: $\lambda = 312° \pm 5°, \beta = -57° \pm 5°$ and $\lambda = 113° \pm 5°$, $\beta = -60° \pm 5°$).

We estimated the Yarkovsky drift for a body of this size, spin and thermal parameters typical for V-type asteroids. We used the derived physical parameters to investigate the origin of

[1] The criterion of a close approach detection was the distance of one Hill radius, defined as $R_{\rm Hill} = a\left(\frac{M_{\rm ast}}{3M_{\rm Sun}}\right)^{\frac{1}{3}}$.

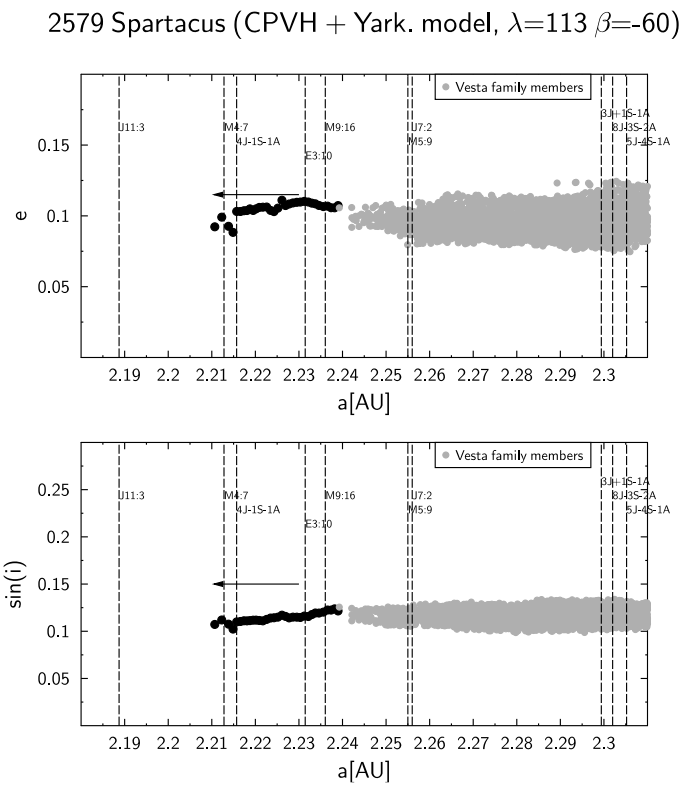

Fig. 8. Evolution of proper elements of Spartacus during 1 Gyr (spin orientation (b)). The direction of the Yarkovsky drift is marked by arrow.

(2579) Spartacus and its link to (4) Vesta. Dynamical integration shows that the asteroid was drifting from the direction of the Vesta family.

We find that at −1 Gyr the asteroid reaches the border of the Vesta family and thus dynamically it is plausible that Spartacus evolved from Vesta, either in the collision that created most of currently observed Vesta family members, or, possibly, in an earlier impact.

Based on spectral observations we find that the band centers are consistent with ranges typical for Vestoids and BAR is roughly half of that of other Vestoids. We analyzed these parameters with rotation and found no surface heterogeneity up to the limit of precision ∼0.3% for band centers and ∼25% for BARs.

In summary, dynamical and physical properties of Spartacus are consistent with origin at Vesta, with the exception of the BAR.

Acknowledgments. First of all, we would like to thank our reviewer Prof. Valerio Carruba for the detailed and insightful comments and suggestions that helped improve our manuscript. This project was supported by the National Science Center, Poland grant number 2017/26/D/ST9/00240. The work of J.Ď. was supported by the grant 18-04514J of the Czech Science Foundation. The work of A.M. was supported by the grant number 2014/13/D/ST9/01818 from National Science Center, Poland. This work is based on obsevations made with the SMARTS telescope (CTIO), Hall telescope (Lowell Observatory), Nordic Optical Telescope and Jacobus Kapteyn Telescope (JKT). The Nordic Optical Telescope is operated by the Nordic Optical Telescope Scientific Association at the Observatorio del Roque de los Muchachos, La Palma, Spain, of the Instituto de Astrofisica de Canarias. The Jacobus Kapteyn Telescope (JKT) is owned by the Southeastern Association for Research in Astronomy (saraobservatory.org). We acknowledge the use of Starlink software which is currently supported by the East Asian Observatory.

References

Asphaug, E. 1997, Meteor. Planet. Sci., 32, 965
Bland, P., Spurnỳ, P., Towner, M., et al. 2009, Science, 325, 1525
Brasil, P., Roig, F., Nesvornỳ, D., & Carruba, V. 2017, MNRAS, 468, 1236
Burbine, T. H., Buchanan, P. C., Binzel, R. P., et al. 2001, Meteor. Planet. Sci., 36, 761
Burbine, T., DeMeo, F., Rivkin, A., & Reddy, V. 2017, Planetesimals: Early Differentiation and Consequences for Planets (Cambridge: Cambridge University Press), 298
Carruba, V., & Nesvornỳ, D. 2016, MNRAS, 457, 1332
Carruba, V., Michtchenko, T. A., Roig, F., Ferraz-Mello, S., & Nesvorný, D. 2005, A&A, 441, 819
Carruba, V., Michtchenko, T., & Lazzaro, D. 2007, A&A, 473, 967
Carruba, V., Huaman, M. E., Domingos, R. C., Santos, C. R. D., & Souami, D. 2014, MNRAS, 439, 3168
Currie, M. J., Berry, D. S., Jenness, T., et al. 2014, in Astronomical Data Analysis Software and Systems XXIII, eds. N. Manset & P. Forshay, ASP Conf. Ser., 485, 391
Cushing, M. C., Vacca, W. D., & Rayner, J. T. 2004, PASP, 116, 362
DeMeo, F. E., Polishook, D., Carry, B., et al. 2019, Icarus, 322, 13
Duffard, R., & Roig, F. 2009, Planet. Space Sci., 57, 229
Dykhuis, M. J., Molnar, L. A., Gates, C. J., et al. 2016, Icarus, 267, 174
Eugster, O., Herzog, G., Marti, K., & Caffee, M. 2006, Meteorites and the Early Solar System II (Tucson: University of Arizona Press), 829
Floss, C., Taylor, L. A., Promprated, P., & Rumble, D. 2005, Meteor. Planet. Sci., 40, 343
Hardersen, P. S., Reddy, V., Cloutis, E., et al. 2018, AJ, 156, 11
Huaman, M. E., Carruba, V., & Domingos, R. C. 2014, MNRAS, 444, 2985
Ieva, S., Dotto, E., Lazzaro, D., et al. 2016, MNRAS, 455, 2871
Ieva, S., Dotto, E., Lazzaro, D., et al. 2018, MNRAS 479, 2607
Kaasalainen, M., & Torppa, J. 2001, Icarus, 153, 24
Kaasalainen, M., Torppa, J., & Muinonen, K. 2001, Icarus, 153, 37
Keel, W. C., Oswalt, T., Mack, P., et al. 2016, PASP, 129, 015002
Klima, R. L., Pieters, C. M., & Dyar:, M. D. 2008, Meteor. Planet. Sci., 43, 1591
Lazzaro, D., Michtchenko, T., Carvano, J., et al. 2000, Science, 288, 2033
Leith, T. B., Moskovitz, N. A., Mayne, R. G., et al. 2017, Icarus, 295, 61
Lord, S. D. 1992, NASA Technical Memorandum 103957
Masiero, J. R., Mainzer, A. K., Grav, T., et al. 2011, ApJ, 741, 68
Mayne, R., Sunshine, J., McSween, Jr., H., Bus, S., & McCoy, T. J. 2011, Icarus, 214, 147
Moskovitz, N. A., & Warner, B. D. 2012, Asteroids, Comets, Meteors 2012, Proceedings of the conference held May 16-20, 2012 in Niigata, Japan. LPI Contribution No. 1667, 6071
Moskovitz, N. A., Lawrence, S., Jedicke, R., et al. 2008, ApJ, 682, L57
Moskovitz, N. A., Willman, M., Burbine, T. H., Binzel, R. P., & Bus, S. J. 2010, Icarus, 208, 773
Nesvorný, D., Roig, F., Gladman, B., et al. 2008, Icarus, 193, 85
Oszkiewicz, D., Kwiatkowski, T., Tomov, T., et al. 2014, A&A, 572, A29
Oszkiewicz, D., Kankiewicz, P., Włodarczyk, I., & Kryszczyńska, A. 2015, A&A, 584, A18
Oszkiewicz, D., Skiff, B. A., Moskovitz, N., et al. 2017, A&A, 599, A107
Rayner, J., Toomey, D., Onaka, P., et al. 2003, PASP, 115, 362
Roig, F., Nesvorný, D., Gil-Hutton, R., & Lazzaro, D. 2008, Icarus, 194, 125
Schenk, P., O'Brien, D. P., Marchi, S., et al. 2012, Science, 336, 694
Scholl, H., & Froeschlé, C. 1991, A&A, 245, 316
Solontoi, M. R., Hammergren, M., Gyuk, G., & Puckett, A. 2012, Icarus, 220, 577
Spoto, F., Milani, A., & Knežević, Z. 2015, Icarus, 257, 275
Spurnỳ, P., Bland, P. A., Shrbenỳ, L., et al. 2012, Meteor. Planet. Sci., 47, 163
Sunshine, J. M., Pieters, C. M., & Pratt, S. F. 1990, J. Geophys. Res. Solid Earth, 95, 6955
Thomas, P. C., Binzel, R. P., Gaffey, M. J., et al. 1997, Science, 277, 1492
Tsirvoulis, G., & Novaković, B. 2016, Icarus, 280, 300
Turrini, D., Svetsov, V., Consolmagno, G., Sirono, S., & Pirani, S. 2016, Icarus, 280, 328
Vokrouhlicky, D. 1998, A&A, 335, 1093
Vokrouhlický, D., & Farinella, P. 1999, AJ, 118, 3049
Wiechert, U., Halliday, A., Palme, H., & Rumble, D. 2004, Earth Planet. Sci. Lett., 221, 373
Yamaguchi, A., Clayton, R. N., Mayeda, T. K., et al. 2002, Science, 296, 334

Appendix A: Additional figures

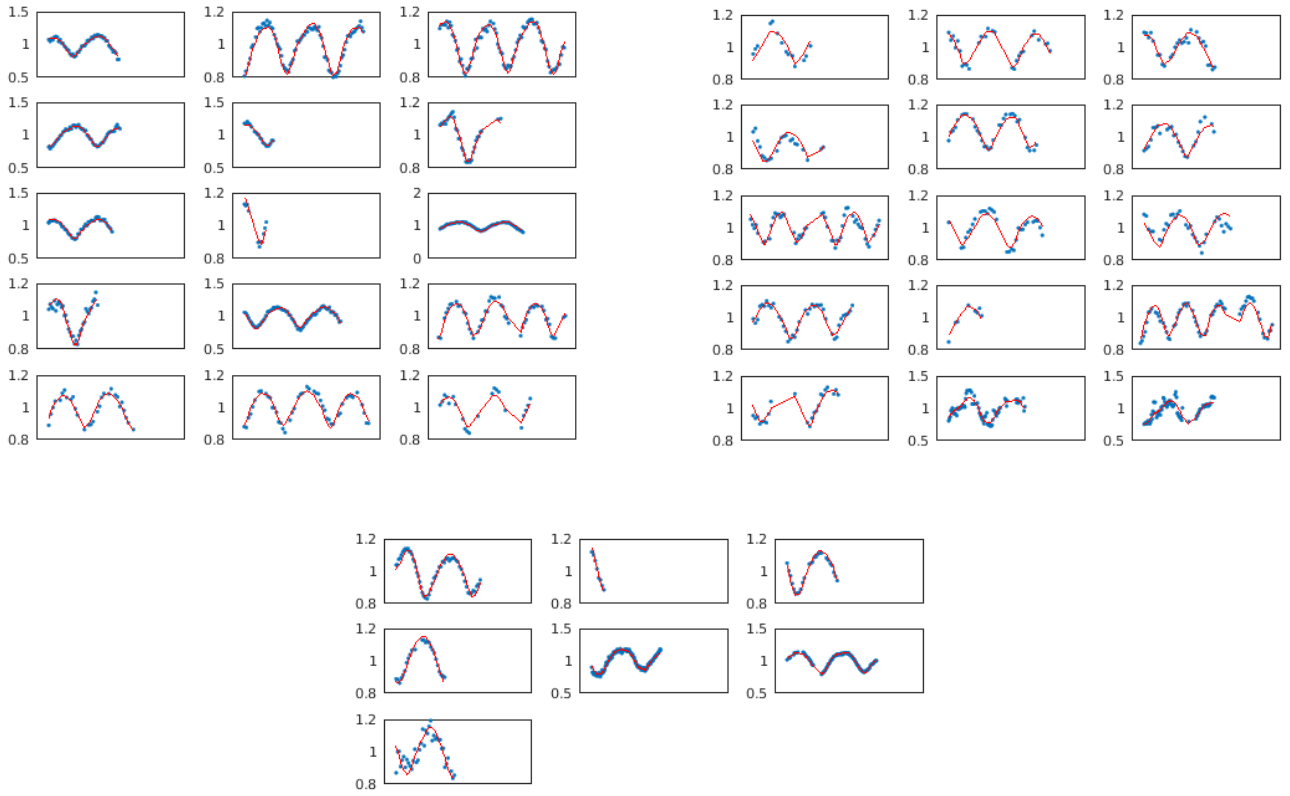

Fig. A.1. Observed lightcurves (blue points) and model solution (solid red line) with pole direction $\lambda = 312°, \beta = -57°$.

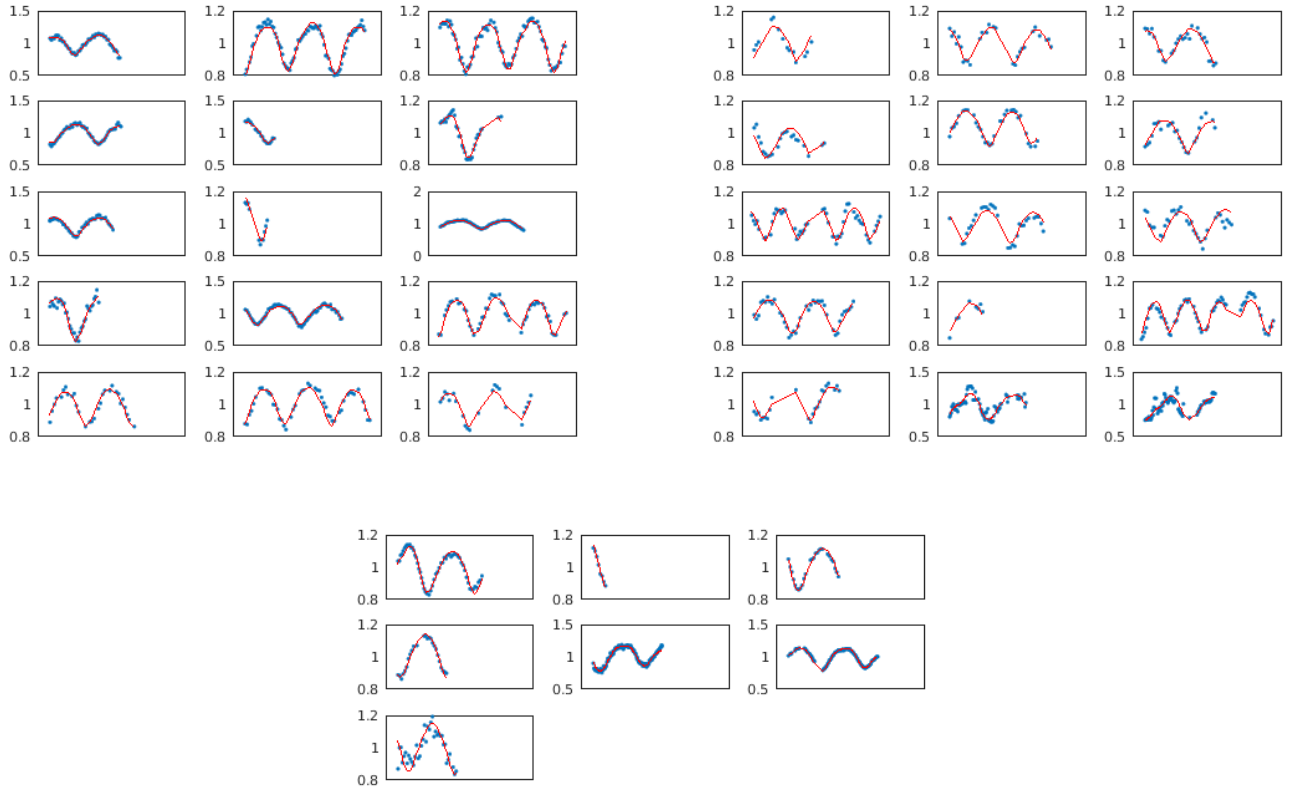

Fig. A.2. Observed lightcurves (blue points) and model solution (solid red line) with pole direction $\lambda = 113°, \beta = -60°$.